Journal of Physics: Conference Series **88** (2007) 012054 doi:10.1088/1742-6596/88/1/012054

Interference of electrons ionized by short laser pulses

D G Arbó [1], S Yoshida [2], E Persson [2], K I Dimitriou [3], and J Burgdörfer [2]

[1] Institute for Astronomy and Space Physics, IAFE, CC67, SUC. 28 (1428) Buenos Aires, Argentina
[2] Institute for Theoretical Physics, Vienna University of Technology, A-1040 Vienna, Austria
[3] Physics Department, National Technical University and National Hellenic Research Foundation, 11635 Athens, Greece

E-mail: diego@iafe.uba.ar

Abstract. We analyze the two-dimensional momentum distribution of electrons ionized by short laser pulses by solving the time-dependent Schrödinger equation. Lindner *et al.*, [Phys. Rev. Lett. **95**, 040401 (2005)] identified oscillations in the electron emission spectrum for ionization by a few-cycle pulse as a time-double slit interference. We extend this analysis to interference fringes in the momentum distributions. For longer pulses we find a complex two-dimensional interference pattern that resembles ATI rings at higher energies and displays Ramsauer-Townsend - type diffraction oscillations in the angular distribution near threshold.

1. Introduction

As increasingly shorter pulses (fs) became available, the interaction of few-cycle laser pulses with matter has attracted considerable interest. Ultrashort pulses with time duration comparable to the optical period lead to novel features of laser-matter interactions. They include the strong carrier-envelope (CE) phase dependence of excitation and ionization processes [1,2]. Electron emission which in the tunnel ionization regime occurs near the extrema of the electric field is temporally confined to a few adjacent field extrema. The interference between such ionization bursts gives rise to features in the electron emission spectrum dP/dE markedly different from the typical above-threshold ionization (ATI) spectrum for longer pulses with well-defined ponderomotive energy [3-8]. Interferences of ultrashort free electron wave packets generated by time delayed femtosecond laser pulses have been observed [9,10]. Lindner *et al.* [11] have recently demonstrated that a single ultrashort pulse with a sine-like envelope gives rise to a double-slit interference in time.

For photodetachment of negative ions classical paths of electrons released in a short-range potential interfere. The interference of electron emission corresponds to that of two laser-induced point sources as in the two-slit Young experiment [12-15]. For neutral rare gases Rudenko *et al.* [5] presented first fully two-dimensional momentum maps for laser-ionized electrons, displaying a complex pattern whose origin was not clear. Since then several theoretical investigations have been performed addressing the interference phenomena involved in atomic ionization by short laser pulses [4,16].

In the present work we firstly extend the study of the time double-slit interference emission pattern to the two-dimensional (2D) momentum distribution of the outgoing electron along the direction of the laser polarization, k_z, and the perpendicular polar coordinate k_ρ. We present full numerical solutions of the time-dependent Schrödinger equation (TDSE). With the help of an analytic semiclassical model

closely following the "simple man's model" (SMM) we analyze the interference fringes in terms of time double-slit interference. Secondly, for longer pulses we find an equally complex yet surprisingly similar pattern suggesting a simple explanation in terms of interferences between different electron trajectories in the combined laser and Coulomb field. The pattern is largely independent of the atomic core potential. Atomic units are used throughout.

2. Theory

We consider an atom in the single electron approximation interacting with a linearly polarized laser field. The Hamiltonian of the system is

$$H = \frac{\boldsymbol{p}^2}{2} + V(r) + zF(t)\,, \tag{1}$$

where $V(r)$ is the atomic potential, $\boldsymbol{p}$ and $\boldsymbol{r}$ are the momentum and position of the electron, respectively, and $F(t)$ is the time dependent external field linearly polarized along the z direction. The laser pulse is chosen to be of the form

$$F(t) \;=\; F_0 \cos^2(\pi t/\tau)\Theta(\tau/2 - |t|)\cos(\omega t + \varphi_{CE})\;\;, \tag{2}$$

where ω is the laser carrier frequency, φ_{CE} the relative carrier-envelope phase, Θ is the Heaviside step function, τ is the total pulse duration and $t = 0$ corresponds to the middle of the pulse. $\varphi_{CE} = 0$ in equation (2) corresponds to a cosine-like pulse while $\varphi_{CE} = \pm\pi/2$ corresponds to a msine pulse.

The time-dependent Schrödinger equation can be solved by means of the generalized pseudo-spectral method [17]. This method combines a discretization of the radial coordinate optimized for the Coulomb singularity with quadrature methods to achieve stable long-time evolution using a split-operator method. It allows for an accurate description of both the unbound as well as the bound parts of the wave function $|\psi(t)\rangle$. The process of detecting an electron of momentum $\boldsymbol{k}$ can then be viewed as a projection of the wave function onto the Coulomb wave functions [18-20]. Therefore, after the laser pulse is turned off, the wave packet is projected onto outgoing Coulomb wave functions, which gives the transition probability

$$dP/d\boldsymbol{k} = \left|T_{if}\right|^2\;\;, \tag{4}$$

with amplitude

$$T_{if} = \frac{1}{\sqrt{4\pi k}} \sum_l e^{i\delta_l(k)} \sqrt{2l+1} P_l(\cos\theta)\;\; \langle k,l\,|\,\psi(\tau)\rangle\;\;, \tag{5}$$

$\delta_l(k)$ is the momentum dependent Coulomb phase shift, θ is the angle between $\boldsymbol{k}$ and the polarization direction of the laser field (chosen along the z-axis), P_l is the Legendre polynomial of degree l, and $\left|k,l\right\rangle$ is the eigenstate of the free atomic Hamiltonian with positive eigenenergy $E = k^2/2$ and orbital quantum number l. Cylindrical symmetry makes the dynamics a two dimensional problem with the projection of the angular momentum on the polarization direction of the laser as constant of motion (the magnetic quantum number m is unaffected during the time evolution). Equation (5) is an acceptable approximation for rare gas atoms since the atomic potential is close to Coulombic for distances larger than a few atomic units [21]: After tunneling, the continuum electron propagates at large distances from the nucleus where the combined laser and asymptotic Coulomb fields dominate.

3. Results

We consider a hydrogen atom initially in its ground state ionized by a pulse with carrier frequency $\omega = 0.05$, peak field $F_0=0.075$ with duration $\tau = 251$ a.u., and $\varphi_{CE} = \pi/2$ (a sine-shaped pulse) which corresponds to a realistic ultrashort pulse containing two optical cycles. For this pulse shape [see inset of Figure 1 (a)], only two paths effectively contribute to the ionization spectrum. The shaded areas in Figure 1 (a) show the two temporal slits where the ionization predominately occurs. The photoelectron spectrum, shown in Figure 1 (a), has a non-equally spaced peak distribution and the separation between two consecutive peaks increases with energy. The peaks correspond to the time-double slit interference fringes observed by Lindner *et al.* [11]. Recent simulations [24] have also shown the existence of these peaks in the density probabilities at different angles of ejection but for a much stronger field (10^{16} Wcm^{-2}) applied to He^+ atoms. The fringe pattern of the doubly-differential momentum distribution $(d^2P/dk_\rho dk_z)$ as a function of the final longitudinal k_z, and transversal momentum of the electron $k_\rho = \sqrt{k_x^2 + k_y^2}$ (Figure 1 (b)) features several characteristics that are noteworthy: (i) the distribution is constrained to the region $-0.5 \lesssim k_z \lesssim 2.5$ and $k_\rho \lesssim 0.6$, (ii) at larger momenta the distribution shows an almost vertical strip-like pattern at larger k_z, slightly bent outward with increasing k_ρ, and (iii) it features a radial-circular nodal pattern near threshold. The fringe pattern can be viewed as a 2D "Ramsey fringe" [25], where the two separated regions of excitation (here ionization) originate from different half-cycles of the same pulse.

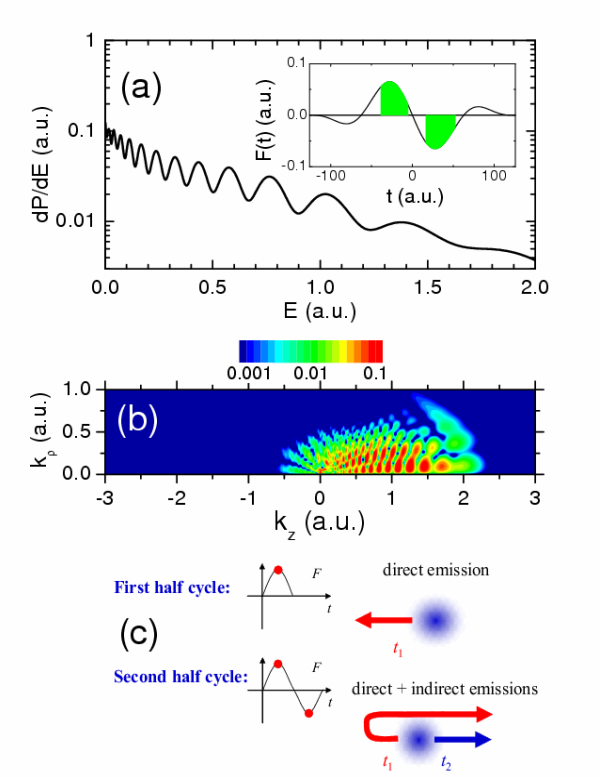

Figure 1. (Color online) (a) Ab initio photoelectron spectra for a two-cycle electric field of frequency $\omega=0.05$ a.u., peak field $F_0=0.075$ a.u. and duration $\tau=4\pi/\omega=251$ (with a $\cos^2$ envelope function) on hydrogen. Inset: Electric field as a function of time. The shaded areas correspond to the two temporal slits. (b) Doubly differential electron momentum distribution (k_z,k_ρ) in logarithmic scale for the same laser pulse. (c) Schematic diagram of the interference process.

In [23] a simple semiclassical model (SMM) [22,24,26] for ultrashort pulses was presented: the diffraction image [Figure 1 (b)] is the result of the superposition of the emission from the atom (point source) into the half-space of positive k_z during the opening of the first temporal slit (t_1) and the beam that is emitted from the point source in opposite direction during the opening of the second temporal slit (t_2) turned around by the field and also emitted in the positive half space [see Figure 1 (c) for a schematic diagram of the process]. The interference pattern is therefore controlled by the phase acquired by the re-directed trajectory during the propagation in the field relative to that of the directly

emitted wave packet. According to the SMM, different trajectories with the same value of the vector potential at the time of detachment interfere [11,23]. For our double-slit photoionization case the interference condition is fulfilled when $t_1 = -t_2$. For the sake of simplicity we consider now a one-cycle –sine pulse with no envelope function. The interference pattern in the photoelectron spectrum [figure 1 (a)] is approximately given by [23]

$$\frac{dP}{dE} \sim A(E)\cos^2\left(\frac{\Delta S(E)}{2}\right), \tag{6}$$

where *A(E)* is a prefactor depending on the electron final energy and *ΔS(E)* is the difference of the accumulated classical action of the two interfering traectories. A Taylor expansion around the energy $E' = F_0^2/2\omega^2$, corresponding to detachment at the maximum and minimum of the 1-cycle pulse ($\Delta t' = t_2 - t_1 = \pi/\omega$) yields

$$\Delta S = \Phi + \Omega(E - E') + \Gamma(E - E')^2, \tag{7}$$

where $\Phi = -\pi F_0^2/4\omega^3$ is an unimportant absolute phase and $\Omega = 2/\omega = (2/\pi)\Delta t'$ near E'. Finally, $\Gamma = -(1+\pi/2)\omega/F_0^2$ controls the negative chirp in the frequency of the energy peaks in the photoelectron spectrum. The energy dependent phase can therefore be written as

$$\Delta S = \Phi + (E - E')\frac{2\Delta t(E)}{\pi}, \tag{8}$$

with

$$\Delta t(E) = \Delta t'\left[1 - (E - E')\left(\frac{1}{2} + \frac{\pi}{4}\right)\frac{\omega^2}{F_0^2}\right].$$

The chirp results in an energy dependent effective width of the double slit *Δt(E)*. In other words, the non-equispaced peaks are due to the slits of varying width (as shown in inset of figure 1 (a)). The accumulated phase of trajectories of slow electrons born at earlier times are considerably larger than that of fast electrons emitted later during the first slit relative to the corresponding to the second slit (for details of the semiclassical description see reference [23]).

Semiclassical models based on the strong field approximation do not reproduce the near threshold structure in the two-dimensional momentum distribution. At low energies the discrepancy is not primarily due to the failure of classical dynamics but is the result of the neglect of the atomic core potential. More pronounced near-threshold patterns occur for longer pulses, i.e., with more than 3 or 4 optical cycles. In figure 2, examples of the two-dimensional momentum distribution for 8-cycles pulses averaged over the CE phase are displayed. In figure 2 (a) the parameters of the field are *ω=0.05*, *τ=1005*, and $F_0 = 0.075$, and the target is H, while in figure 2 (b) *ω=0.057, τ=882* and $F_0 = 0.065$ and the target is Ar. Both momentum distributions display a complex interference pattern which is characterized by a transition from a ring-shaped pattern at larger $k = \sqrt{k_\rho^2 + k_z^2} > 0.4$ with circular nodal lines to a very different pattern of pronounced radial nodal lines for small k near threshold. The first point to be noted is that the overall pattern displays a surprising and striking similarity to the experimental pattern observed recently for rare gases [5,27]. The ring pattern is reminiscent of ATI peaks of the multi-photon regime.

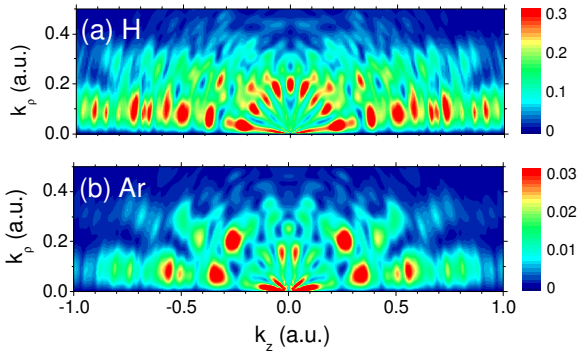

Figure 2. (Color online) Doubly-differential electron momentum distributions of (a) H with parameters of the field $\omega=0.05$, $\tau=1005$, and $F_0=0.075$ and (b) Ar with $\omega=0.057$, $\tau=882$ and $F_0=0.065$. An average over the CE phase was performed.

The doubly-differential momentum distribution with fixed CE phase $\varphi_{CE} = 0$ displays a very pronounced near-threshold structure with a bouquet shape [Figure 3 (a)]. Radial lines indicate the position of the nodal lines (minima) of the angular distribution. The number of minima in this case is eight. The distribution of contributing partial waves p_l is presented in figure 3 (b) for the first and second ATI rings as indicated in the figure. The partial-wave distribution near threshold peaks at $l_0=8$, which is enhanced by the relative suppression of adjacent angular momentum $l_0 \pm 1$ of opposite parity remnant of the multi-photon parity selection rule. The second ring shows a maximum at $l_0=9$, even though no dominance of a single partial wave is evident when looking at the angular distribution (not shown). According to equation (5) the dominance of a single partial wave in the momentum-differential ionization cross section implies the dominance of a single Legendre polynomial:

$$\frac{d^2P}{d\boldsymbol{k}} \propto \left[P_{l_0}(\cos\theta)\right]^2. \tag{9}$$

Since the number of zeros of the dominant Legendre polynomial is equal to the dominant angular momentum l_0, equation (9) predicts the number of nodal lines to be l_0, as observed in Figures 3 (a) and (b).

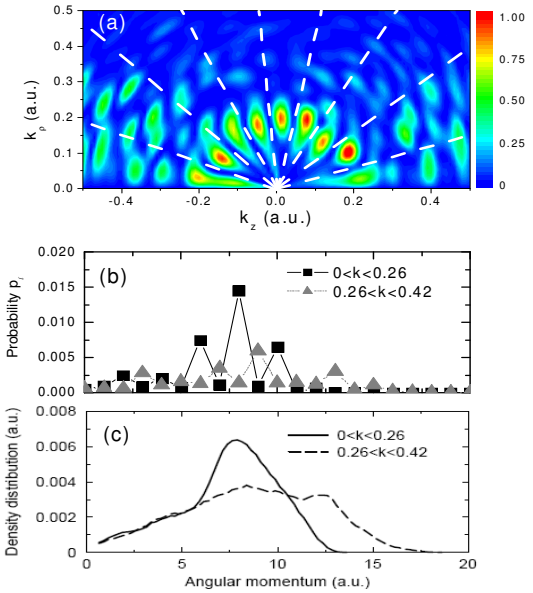

Figure 3. (Color online) (a) Doubly-differential electron momentum distributions for H. (b) Partial ionization probability p_l as a function of the angular momentum l for the different spectral regions indicated in the figure. (c) Angular momentum distribution of classical trajectories. The parameters of the field are $\omega=0.05$, $\tau=1005$, and $\gamma=0.67$ ($F_0=0.075$).

A simple semiclassical analysis of the interference pattern in the angular distribution can be performed. To uncover the relevant classical paths we employ a CTMC-T simulation [3] for the same parameters as in figure 3. The ensemble of ionized electrons near threshold features, indeed, an L distribution [figure 3 (c)] that resembles the quantum distribution (figure 3) with a peak near $l_0=8$, clearly emphasizing the underlying classical character of this process. A typical electron trajectory after tunneling shows a quiver motion along the polarization of the laser field. Even though the motion is strongly driven by the laser field, the motion follows the Kepler hyperbola [figure 4 (a) and (b)] if the atomic potential can be approximated by a purely Coulombic one. The point to be emphasized is that the dashed line in the figure 4 (a) and (b) does not represent the laser-driven trajectory averaged over a quiver oscillation period but the unperturbed Kepler hyperbola with the identical asymptotic momentum as the laser driven trajectory (solid line). Thus, the angular momentum of the Kepler hyperbola is identical to that of the asymptotic L of the laser-driven electron. Identifying the pericenter of the hyperbola with the quiver amplitude, $\alpha = \left[\sqrt{Z^2 + (kL)^2} - Z\right]/k^2$ with $\alpha = F_0/\omega^2$, results in a simple relation between the angular momentum L and α [28],

$$L(k) = (2Z\alpha)^{1/2}\left(1+\frac{\alpha^2 k^2}{2Z}\right)^{1/2}. \qquad (10)$$

This simple classical formula predicts the number of quantum interference minima or the peak in the calculated partial wave populations. The initial conditions for the laser driven trajectory are provided by tunneling ionization with the release of the electron with zero longitudinal velocity at times t_i near the maxima of the field amplitude $F(i_t) \simeq F_0$. Note that the number of quiver oscillations along the Kepler orbit is not unique thus allowing for path interferences. Trajectories released at different times t_i or different maxima of the field reaching the same asymptotic branch of the Kepler hyperbola will interfere and generate generalized Ramsauer-Townsend (GRT) interference fringes [4,29]. In order to reach the limiting case of the dominance in the semiclassical domain of a single P_{l_0} it is necessary that interference trajectories at fixed energy that approximately cover the entire range of scattering angles $(0 \lesssim \theta \lesssim \pi)$ all of which with angular momenta close to l_0 exist. Our CTMC-T calculations show that close to threshold such families of trajectories indeed exist [4]. Analogous path interference occurs in electron-atom scattering where GRT interference fringes can be semiclassically described in terms of interferences of paths with different angular momenta scattered into the same angle [29].

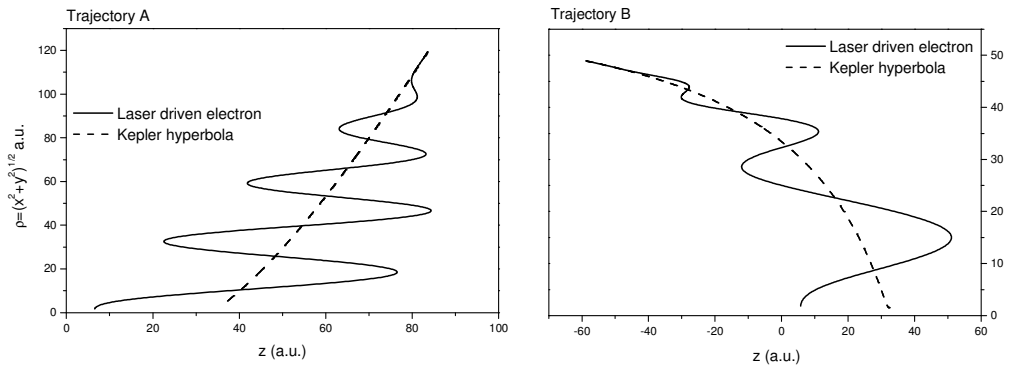

Figure 4. Classical trajectories of laser-driven electrons (solid lines) and unperturbed Kepler hyperbola of same asymptotic E and L (dashed lines).

At threshold, i.e., $k = 0$, Equation (10) reduces to: $L = \sqrt{2Z\alpha}$, which depends only on the quiver amplitude (i.e. the laser parameters) and the charge of the (asymptotic) Coulomb field Z. In figure 5 we plot the dominant angular momenta L, i.e., the number of nodal lines near the origin, as a function of the quiver amplitude α for different atomic species (H, Ar, Kr, Ne, He) from theoretical calculations [4,14,16,30]. Very good agreement to our predictions is observed without any adjustable parameters.

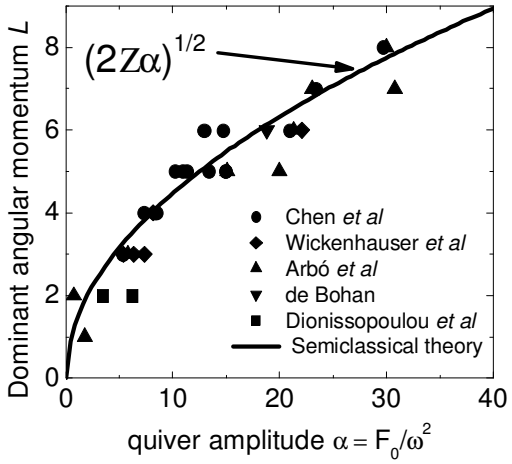

Figure 5. Dominant angular momentum as a function of the quiver amplitude. The semi-classical estimate (solid line) is compared with different quantum simulations: Chen *et al.* [16] (circles), Wickenhauser et al [30] (rhombus), Arbó *et al.* [4] (up triangles), de Bohan [31] (down triangles), and Dionissopouplou *et al.* [18] (squares).

4. Conclusions

We have presented theoretical studies of the interference effect observed in the electron distributions of ionized atoms subject to linearly polarized ultrashort laser pulses. We have extended the previous analysis in the energy domain to the full two-dimensional momentum space distribution. After one- and two-cycle pulses, the two-dimensional electron momentum distribution displays interference fringes identified as interference between the wave packets released during the first and second half cycle. Each half cycle operates as an independent slit. For a multi-cycle pulse the near-threshold pattern has been recently analyzed in terms of generalized Ramsauer-Townsend diffraction oscillations [4], where Coulomb scattering effects have been shown to be important. A simple semiclassical analysis identifies the fringes resulting from interfering paths released at different times but reaching the same Kepler asymptote. The present result shows that a proper semiclassical description along the lines of the "simple man's model" [32] requires the inclusion of Coulomb scattering. Our results feature a striking similarity to recent data by Rudenko *et al.* [5] suggesting the presence of the 2D interference fringes to be mostly independent of the specific atomic species.

Acknowledgements

This work was performed with financial support of CONICET of Argentina, by the SFB 016 ADLIS and the project P15025-N08 of the FWF (Austria), and by EU project HPRI-CT-2005-026015.

References

[1] Paulus G G, Grasbon F, Walther H, Villoresi P, Nisoli M, Stagira S, Priori E and De Silvestri S 2001 *Nature* (London) **414**, 182
[2] Martiny C P J and Madsen L B 2006 *Phys. Rev. Lett.* **97**, 093001
[3] Dimitriou K I, Arbó D G, Yoshida S, Persson E and Burgdörfer J 2004 *Phys. Rev. A* **70**, 061401(R)
[4] Arbó D G, Yoshida S, Persson E, Dimitriou K I and Burgdörfer J 2006 *Phys. Rev. Lett.* **96**, 143003
[5] Rudenko A, Zrost K, Schröter C D, de Jesus V L B, Feuerstein B, Moshammer R and Ullrich J 2004 *J. Phys. B* **37**, L407

[6] Maharjan C M, Alnaser A S, Litvinyuk I, Ranitovic P and Cocke C L 2006 *J. Phys. B* **39**, 1955
[7] Faisal F H M and Schlegel G 2005 *J. Phys. B* **38**, L223
[8] Chen J, Liu J, Fu L B, and Zheng W M 2000 *Phys. Rev. A* **63**, 011404(R)
[9] Wollenhaupt M, Assion A, Liese D, Sarpe-Tudoran Ch, Baumert T, Zamith S, Bouchene M A, Girard B, Flettner A, Weichmann U and Gerber G 2002 *Phys. Rev. Lett* **89**, 173001
[10] Wollenhaupt M, Präkelt A, Sarpe-Tudoran Ch, Liese D and Baumert T 2005 *J. Opt. B: Quantum Semiclass. Opt*. **7**, S270-S276
[11] Lindner F, Schätzel M G, Walther H, Baltuška A, Goulielmakis E and Krausz F 2005 *Phys. Rev. Lett.* **95**, 040401
[12] Krajewska K, Fabrikant I I and Starace A F 2006 *Phys. Rev. A* **74**, 053407
[13] Reichle R, Kiyan I Y and Helm H P 2003 *Jour. Modern Optics* **50**, 461
[14] Reichle R, Helm H P and Kiyan I Y 2003 *Phys. Rev. A* **68**, 063404
[15] Gribakin G F and Kuchiev M Y 1997 *Phys. Rev. A* **55**, 3760
[16] Chen Z, Morishita T, Le A-T, Wickenhauser M, Tong X-M and Lin C D 2006 *Phys. Rev. A* **74**, 053405
[17] Tong X-M and Chu S I 1997 *Chem. Phys.* **217**, 119
[18] Dionissopoulou S, Mercouris Th, Lyras A and Nicolaides C A 1997 *Phys. Rev. A* **55**, 4397
[19] Schöller O, Briggs J S and Dreizler R M 1986 *J. Phys. B* **19**, 2505
[20] Messiah A 1965 *Quantum Mechanics 1* (New York: North-Holland)
[21] Muller H G 1999 *Phys. Rev. A* **60**, 1341
[22] Chirila C C and Potvliege R M 2005 *Phys. Rev. A* **71**, 021402(R)
[23] Arbó D G, Persson E and Burgdörfer J 2006 *Phys. Rev. A* **74**, 063407
[24] Delone N B and Krainov V P 1991 *J. Opt. Soc. Am. B* **8**, 1207
[25] Scully M O and Zubairy M S 1997 *Quantum Optics* (New York: Cambridge U. P., p. 550)
[26] Lewenstein M, Kulander K C, Schafer K J and Bucksbaum P H 1995 *Phys. Rev. A* **51**, 1495
Lewenstein M, Balcou Ph, Ivanov M Y, L'Huillier A and Corkum P B 1994 *Phys. Rev. A* **49**, 2117
[27] Maharjan C M, Alnaser A S, Litvinyuk I, Ranitovic P and Cocke C L 2006 *J. Phys. B* **39**, 1955
[28] Landau L D and Lifshitz E M 1960 *Mechanics* (Oxford: Pergamon Press)
[29] Burgdörfer J, Reinhold C, Sternberg J and Wang J 1995 *Phys. Rev. A* **51**, 1248
[30] Wickenhauser M, Tong X-M, Arbó D G, Burgdörfer J and Lin C D 2006 *Phys. Rev. A* **74**, 041402(R)
[31] de Bohan A, Ph.D. thesis 2001, Université Catholique de Louvan
[32] Corkum P B, Burnett N H and Ivanov M Y 1994 *Opt. Lett.* **19**, 1870
Ivanov M, Corkum P B, Zuo T and Bandrauk A 1994 *Phys. Rev. Lett.* **74**, 2933